


ORIGINAL ARTICLE

Structural variations in hyperbranched polymers prepared via thermal polycondensation of lysine and histidine and their effects on DNA delivery

Ali Alazzo,^{1,2} Tatiana Lovato,¹ Hilary Collins,¹ Vincenzo Taresco,¹ Snjezana Stolnik,¹ Mahmoud Soliman,³ Keith Spriggs¹ & Cameron Alexander^{1*} 

¹ School of Pharmacy, University of Nottingham, Nottingham NG7 2RD, UK

² Department of Pharmaceutics, University of Mosul, Mosul, Iraq

³ Department of Pharmaceutics, Ain Shams University, Cairo, Egypt

Keywords

gene delivery, histidylated polymers, hyperbranched polymers, thermal polycondensation.

Correspondence

Cameron Alexander, School of Pharmacy, University of Nottingham, Nottingham, NG7 2RD, UK.

Tel: +44 (0)115 846 7678

Email: cameron.alexander@nottingham.ac.uk

FUNDING INFORMATION

Engineering and Physical Sciences Research Council, EP/H005625/1;

Royal Society Wolfson Research Merit Award, WM150086;

Higher Committee for Education Development in Iraq

Received: 12 February 2018;

Revised: 27 February 2018;

Accepted: 21 March 2018

Journal of Interdisciplinary
Nanomedicine,

2018; 3(2), doi: 10.1002/jin2.36

Abstract

The successful clinical translation of nonviral gene delivery systems has yet to be achieved owing to the biological and technical obstacles to preparing a safe, potent, and cost-effective vector. Hyperbranched polymers, compared with other polymers, have emerged as promising candidates to address gene delivery barriers owing to their relatively simple synthesis and ease of modification, which makes them more feasible for scale-up and manufacturing. Here, we compare hyperbranched poly(amino acids) synthesised by copolymerising histidine and lysine, with hyperbranched polylysine prepared using the well-known “ultrafacile” thermal polycondensation route, to investigate the effects of histidine units on the structure and gene delivery applications of the resultant materials. The conditions of polymerisation were optimised to afford water-soluble hyperbranched polylysine-co-histidine of three different molar ratios with molecular masses varying from 13 to 30 kDa. Spectroscopic, rheological, and thermal analyses indicated that the incorporation of histidine modulated the structure of hyperbranched polylysine to produce a more dendritic polymer with less flexible branches. Experiments to probe gene delivery to A549 cells indicated that all the new hyperbranched polymers were well tolerated, but, surprisingly, the copolymers containing histidine were not more effective in transfecting a luciferase gene than were hyperbranched polylysines synthesised as established literature comparators. We attribute the variations in gene delivery efficacy to the changes induced in polymer architecture by the branching points at histidine residues, and we obtain structure-function information relating histidine content with polymer stiffness, pKa, and ability to form stable polyplexes with DNA. The results are of significance to nanomedicine design as they indicate that addition of histidine as a co-monomer in the synthetic route to hyperbranched polymers not only changes the buffering capacity of the polymer but has significant effects on the overall structure, architecture, and gene delivery efficacy.

Introduction

The development of safe, efficient, and cost-effective vectors for gene delivery remains a challenge for research scientists, industrial developers, and clinicians alike. This is mainly due to the biological and technical barriers that prevent delivery of exogenous therapeutic biomolecules. Efficient gene vectors should protect the nucleic acid from enzymatic degradation during transit in the body, facilitate accumulation at target organs and avoid off-target toxicity, and be able to enter cells and escape intracellular compartments to deliver their payload where needed (Keles et al., 2016, Kanasty et al., 2013, Islam et al., 2015, Wagner, 2013). In addition, gene delivery vectors should be adaptable to pharmaceutical manufacturing and scale-up protocols (Zhang et al., 2013), which can be significant barriers to clinical adoption of complex nanomedicines.

Nonviral vectors are primarily cationic materials that condense negatively charged nucleic acids into polyelectrolyte complexes (Samal et al., 2012, Kudsiova et al., 2016, Hurley et al., 2008). They have the ability to interact electrostatically with the negative charge of nucleic acids and condense them into nanoparticles (De Smedt et al., 2000, Oupicky et al., 2000). These vectors offer advantages over viral vectors in immunogenicity and carcinogenicity, packing capacity, and possibility for scale-up, even if many early examples exhibited lower transfection efficiency with transient gene expression and relatively high cytotoxicity (Godbey et al., 2001). More recent studies have utilised a very wide variety of functionalised cationic lipids (Viricel et al., 2017, Altnoglu et al., 2016, Semple et al., 2010) and cationic polymers, with increasing efficacy in transfecting target cells with reduced toxicity (Luo et al., 2017, Blum et al., 2016, Lee et al., 2015, Cho et al., 2015). In this context, polymers based on polyamidoamine, polyethylenimine (PEI), and polylysine (PLL), synthesised into varying architectures from linear to branched and dendritic, have been designed and developed as efficient gene carriers (Khandare et al., 2012, Ainalem et al., 2009, Dufes et al., 2005, Hardy et al., 2009, Bansal et al., 2015, Sun and Davis, 2010). However, the syntheses of some of these materials are difficult to scale up, rendering the pharmaceutical applications of such materials more difficult.

In order to overcome the cost and scale-up issue, hyperbranched polymers have been considered as alternatives to precisely synthesise block copolymers and dendrimers. Hyperbranched polymers have similar properties to dendrimers, and although polydisperse,

the Klok group in particular has shown that hyperbranched PLLs (*hb*-polyK) can be prepared in “one-pot” reactions, making them more amenable to scale up and industrial manufacturing (Scholl et al., 2009). *hb*-polyK is a biocompatible and biodegradable polycation and can be synthesised through thermal polymerisation of amino acids without any protection and/or preactivation of monomer (Scholl et al., 2009). During this polymerisation, no organic solvents are needed, and the fact that lysine is a renewable material that can be obtained by fermentation routes (Chen et al., 2014) means that polycations obtained in this way can be considered to be sustainable on the basis of the principles of green chemistry. In terms of scalability, it has been shown that *hb*-polyK synthesised in this way has several advantages over linear and dendritic PLL gene carriers (Kadlecova et al., 2012b, Kadlecova et al., 2013, Kadlecova et al., 2012a). In addition, polyamides have the advantage of being biodegradable (Kodama et al., 2014, Leclercq et al., 2010), thus reducing their duration of time in the body and any potential build-up in either tissue or the environment following excretion.

The practical utility of the Klok group route to *hb*-polyK materials is highly promising, but one potential drawback is that some PLL preparations have been reported to be cytotoxic and also less effective in transfecting cells than the widely used nonviral vector PEI. Functionalisation of PLLs, by reaction with histidine derivatives, have been shown to increase transfection efficiencies (Soliman et al., 2012, Nasanit et al., 2008). This enhancement has been attributed to the ability of the histidine units to become protonated in endosomal compartments (Midoux et al., 2009) and thus to behave as a “proton sponge” in a manner analogous to that reported for PEI. However, the routes to these histidine-functionalised PLLs can be complex, and there is a clear practical incentive to adapt the more simple, and also well-established, thermal polycondensation of lysine to include the co-monomer histidine and thus generate the polylysine-co-histidine polymers in one step. We accordingly report here the synthesis of hyperbranched polylysine-co-histidine (*hb*-polyKH) via a modification of the Scholl route (Scholl et al., 2007b) and evaluate the resultant polymers against *hb*-polyK materials, as well-studied comparators, in gene delivery studies. We show that addition of histidine into the thermal polycondensation generates materials with a higher buffer capacity than those of *hb*-polyK, but also with a more rigid structure

and dendritic architecture. In turn, these changes in the polymer architecture reduce the stability of poly-electrolyte complexes with DNA at lower cation : anion ratios and lower the DNA transfection efficiency in a cancer cell line.

Experimental

Materials

Lysine-monohydrochloride (lysine-HCl), histidine, PEI, and all buffers and solvents were purchased from Sigma-Aldrich (Gillingham, UK) unless otherwise stated. Agarose, Coomassie Blue, ethidium bromide, fluorescamine, deuterium oxide, and sodium hydroxide were obtained from Fisher Scientific (Loughborough, UK). Fluorescein isothiocyanate (FITC), potassium hydroxide (KOH), methylthiazolyldiphenyl-tetrazolium bromide (MTT), and all routine cell culture materials, Hoechst and Accutase solution were received from Sigma-Aldrich (Gillingham, UK). Calf thymus DNA and LysoTracker Green DND-26 were obtained from Thermo Fisher Scientific (Loughborough, UK), luciferase reporter plasmid (gWiz-Luc) from Aldevron (North Dakota, USA), jetPRIME® from Polyplus Transfection (Illkirch, France), and Spectra/Por dialysis membrane (molecular weight cut-off 1000 Da) from Spectrum Labs (Waltham, USA). Blue/orange-loading dye (6×) and luciferase assay kit were purchased from Promega Corporation (Madison, USA).

Synthesis of hyperbranched polylysine

Hyperbranched polylysine was prepared by thermal polymerisation of lysine-HCl monomers as reported by Scholl et al. (2007b). In a round-bottom flask, lysine-HCl (27.3 g, 0.15 mol) was dissolved in 30 mL of deionised water and neutralised by 8.4 g (0.15 mol) of KOH. The flask was connected to nitrogen stream and heated to 150°C under continuous mechanical stirring. The reaction was carried out up to 48 h; then the crude product of the reaction was dissolved in 10-20 mL of 0.06 N HCl and dialysed using dialysis membrane of molecular mass cut-off 1000 Da, against water (3500 mL × five changes) for two days. The polymer subsequently was freeze-dried and stored at -20°C. Characterisation data shown subsequently were in accord with the previous reports for *hb*-polyK (Scholl et al., 2007b).

Fourier-transform infrared (FT-IR; /cm): 3283, 3063, 2925, 2862, 1644, 1529, 1439, 1369, 1309, 1253. ¹H-NMR (400 MHz, D₂O) δ = 4.13 (b, 1H, COCH(R)N _{α} H,

dendritic unit), 3.85 (br, 1H, COCH(R)N _{α} H, α -linear unit), 3.33 (br, 1H, COCH(R), terminal unit), 3.23 (br, 1H, COCH(R)N _{α} H, ϵ -linear unit), 3.11 (br, 2H, -CH₂-N _{ϵ} H), 2.68 (br, 2H, -CH₂-N _{ϵ} H₂), 1.8-1.2 (br, 6H, -CH₂-). ¹³C-NMR (100 MHz, D₂O) δ = 177.3 (-C(O)-NH), 54.6 (-COCH(R)N _{α} H), 38.9 (-CH₂-N _{ϵ} H₂), 34.0 (-CH₂-CH-N _{α} H₂), 28.2 (-CH₂-CH₂-N _{ϵ} H), 22.3 (-CH₂-CH₂-CH₂-N _{ϵ} H₂).

Synthesis of hyperbranched polylysine-co-histidine

The same procedure used to prepare *hb*-polyK was adapted for the synthesis of *hb*-polyKH. Varying amounts of histidine (corresponding to lysine : histidine molar ratios of 10:1, 2, and 4) were dissolved with 27.4 g lysine-HCl (0.15 mol), in 30 mL of water, followed by neutralisation of the solution with 8.4 g (0.1 mol) of KOH. The solution was heated to 150°C under a nitrogen stream with continuous stirring using an overhead stirrer up to 48 h. Then the reaction was stopped and the product was dissolved in 10-20 mL of 0.06 N HCl, dialysed for two days, and then freeze-dried. The product was stored in a freezer at -20°C.

FT-IR (/cm): 3283, 3074, 2929, 2892, 1640, 1529, 1443, 1369, 1309, 1253. ¹H-NMR (400 MHz, D₂O) δ = 7.59 (br, 1H, CH of imidazole ring), 6.81 (br, 1H, CH of imidazole ring), 4.11 (br, 1H, COCH(R)N _{α} H, dendritic unit), 3.85 (br, 1H, COCH(R)N _{α} H, α -linear unit), 3.31 (br, 1H, COCH(R)N _{α} H₂, terminal unit), 3.22 (br, 1H, COCH(R)N _{α} H, ϵ -linear unit), 3.10 (br, 2H, -CH₂-N _{ϵ} H), 2.77 (br, 2H, -CH₂-N _{ϵ} H₂), 1.8-1.2 (br, 6H, -CH₂-). ¹³C-NMR (100 MHz, D₂O) δ = 177.3 (C(O)-NH), 135.8 (C of imidazole ring), 54.6 (COCH(R)N _{α} H), 38.9 (-CH₂-N _{ϵ} H₂), 34.0 (-CH₂-CH₂-N _{α} H₂), 28.28 (-CH₂-CH₂-N _{ϵ} H), 22.38 (-CH₂-CH₂-CH₂-N _{ϵ} H₂).

Fluorescein labelled hyperbranched polymers

Fluorescein isothiocyanate was used to label the obtained hyperbranched polymers. From a freshly prepared solution of FITC in anhydrous dimethyl sulfoxide (1 mg/mL), aliquots equivalent to 1% of amines in each polymer were added slowly to the polymer solutions (2-4 mg/mL in 0.1 M sodium bicarbonate buffer, pH 9) with continuous stirring for 2 h at room temperature, and then the reactions solutions were left overnight in the fridge. The products were purified by dialysis (molecular weight cut-off 1000 Da) against deionised water for two days. After that, the labelled polymers were recovered using freeze-dryer and stored in a freezer at -20°C.

Polymer characterisation

$^1\text{H-NMR}$ and $^{13}\text{C-NMR}$ experiments were performed using a DPX400 Ultrashield spectrometer (from Bruker, UK). The chemical shifts were recorded as parts per million (δ) relative to the referenced shifts of residual solvent resonances. All the samples were prepared in deuterium oxide at concentrations of 5–10 mg/mL (30–40 mg/mL for $^{13}\text{C-NMR}$). The following abbreviations have been used to report the spectra: s = singlet, br = broad, d = doublet, t = triplet, and m = multiplet. Aqueous gel permeation chromatography was performed using a 1260 Infinity GPC/SEC System from Agilent Technologies (California, USA) adapted with a multiple-angle light scattering detector in addition to differential refractive index and UV-vis detector. A solution of 1 M acetic acid and 0.3 M disodium phosphate (pH 3) was used as eluent, with a flow rate of 1 mL/min. Infrared spectra were measured using a Cary 630 Microlab FT-IR software from Agilent Technology (California, USA). Thermal analysis was carried out on a differential scanning calorimetry Q200 from TA Instruments (New Castle, USA). The rheological measurements were performed using Physica Rheometer (from Anton Paar, Austria), equipped with parallel plate geometry (25-mm diameter), and the gap distance between two plates was set as 0.5 mm. RHEOPLUS software, version 3.6x (from Anton Paar, Austria), was used for analysing data.

Determination of branching parameters

The degree of branching (DB) was calculated as described by Hawker et al. (1991) using the equation

$$DB = D + T/D + L + T$$

while for the average number of branches (ANB), the following equation was used, as suggested by Hölter et al. (1997):

$$ANB = D/D + L$$

where D , T , and L are the mole fraction of dendritic, terminal, and linear units of the hyperbranched polymer, respectively. In both equations, the mole fraction of structural units was determined on the basis of the integration of corresponding peaks of the $^1\text{H-NMR}$ spectrum using MESTRENOVA (v 5.2.5) software from Mestrelab Research (Spain).

Potentiometric titration

Acid-base titration was performed using a Fisherbrand pH meter with Hydrus 600 electrode (Loughborough,

Structural variations in hyperbranched polymers

UK). The samples were prepared by dissolving the polymers in 0.1 M NaCl at a concentration of 1 mg/mL. The pH was adjusted to be in range of 2–3 using 0.1 M HCl and then titrated manually using 0.1 M NaOH up to pH 11. The buffer capacity of the samples was defined as the percentage of ionised amine groups from pH 5 to 7 and calculated on the basis of the following equation (Zhong et al., 2005):

$$\text{Buffer capacity}(\%) = 100 (\Delta V_{\text{NaOH}} \times 0.1 \text{ M}) / N_{\text{mol}}$$

where ΔV_{NaOH} is the volume of 0.1 M NaOH, which changes the pH of the polymer sample from 5 to 7, and N_{mol} is the total moles of amine groups in the sample.

Fluorescamine assays for amine content determination

The intensity of fluorophore resulting from the reaction of fluorescamine with primary amine was measured using a Cary Eclipse Fluorescence Spectrophotometer (ThermoFisher, UK) and glycine as standard. To a 2 mL sample of polymer solution (concentration 2.5 $\mu\text{g/mL}$, in borate buffer pH 8.7), 0.5 mL of fluorescamine in acetone (0.3 mg/mL) was added and vortexed for 10 sec. After incubation of the reagents in the dark for 20 min, the emission from the resulting solution was measured at a wavelength of 480 nm using an excitation wavelength of 385 nm against a blank of borate buffer with fluorescamine, and the sensitivity control of the spectrofluorimeter was fixed at 5.

Preparation of polyplexes

The complexes of polymers with DNA were prepared in two types of buffer (10 mM HEPES and phosphate-buffered saline (PBS)) of pH 7.4. In both conditions, 100 μL containing 5 μg of DNA (calf thymus DNA) or luciferase reporter plasmid (gWiz-Luc), which was used as received without any further purification, was mixed with 100 μL of the polymer solution at concentrations equivalent to N/P ratios of 0.5, 1, 2, 3, 5, 10, and 20. The N/P ratio was calculated on the basis of the results of a fluorescamine assay.

Particles size and zeta potential

The hydrodynamic radii of prepared polyplexes (as described earlier) were measured using a Viscotek 802 supported by OMNISIZE 0.3 V software (UK). All measurements were carried out at a scattering angle of 90° and a temperature of 25°C . For zeta potential, the

prepared polyplexes were diluted to 1 mL using 5 mM NaCl, and measurements were performed using a Malvern Zetasizer (Malvern, UK).

Atomic force microscopy

Polyplexes prepared at N/P ratio of 5 in HEPES buffer (10 mM, pH 7.4) were used for atomic force microscopy (AFM) imaging using mica as a support disc. The specimens were prepared by depositing 100 μ L of polyplexes solution on freshly cleaved mica for 30 sec, then the excess of solution was removed, and the samples were washed twice with 200 μ L of HEPES buffer. Samples were dried using a dry filtered air for 5 min before being imaged in air. A FastScan AFM (from Bruker Nano, UK) was used throughout this study. The cantilevers, used for imaging in air using and Peak Force Tapping mode, were Tap150A with a spring constant of 5 N/m operating at resonant frequencies of approximately 150 kHz. Images were analysed by using the computer software NANOSCOPE software version 7.3 (from Veeco, USA).

Agarose gel electrophoresis with Coomassie Blue staining

For gel preparation, agarose in Tris-acetate-EDTA buffer (0.7%) was heated, using a microwave, for 2 min until a clear solution was obtained. The solution was cooled in a water bath at 55°C. Then, it was mixed with 20 μ L of 10 mg/mL of ethidium bromide and cast into a sealed electrophoresis tray containing the appropriate combs. The gel was allowed to set before it was submerged in an electrophoresis chamber containing 0.5-1 L of Tris-acetate-EDTA buffer. The samples were prepared by adding 5 μ L of the loading dye to 25 μ L of polyplexes, prepared using calf thymus DNA, and the gel was run for 1 h at 70 V. The results were seen and recorded using UV-transilluminator (from Syngene, Germany). Coomassie Blue (0.1% w/v Coomassie Blue in a 50:10:40 solution of methanol/glacial acetic acid/water) was used to stain the gel. After 1 h, the staining solution was removed and replaced by destained solution (methanol/glacial acetic acid/water solution at ratio of 10:10:80) for 24 h.

Ethidium bromide displacement assay

In this assay, calf thymus DNA (50 μ g/mL in PBS) was incubated with ethidium bromide (2 μ g/mL) for 30 min. After that, aliquots of 100 μ L were mixed with 100 μ L of polymer solutions at concentrations equivalent to the different N/P ratios. The samples were left for another 30 min, and then the fluorescence intensity of

DNA-ethidium bromide complexes was measured at a wavelength of 590 nm using an excitation wavelength of 520 nm.

Cell culture

All the biological tests were conducted using A549 cells (human adenocarcinomic alveolar basal epithelial, ATCC® CCL-185) and H1299 (human non-small cell lung carcinoma, ATCC CRL-5803) from ATCC (Manassas, Virginia, USA). The cells were cultured in Dulbecco's modified Eagle's medium (DMEM) and Roswell Park Memorial Institute medium (RPMI), respectively, supplemented with 10% foetal bovine serum (FBS) and 1% L-glutamic acids under a humidified atmosphere containing 5% CO₂ and used in passage number of 30-40.

Metabolic activity (MTT) assay

Into a 96-well plate, 5000 A549 cells/well were seeded and incubated in 100 μ L of DMEM supplemented with 10% FBS and 1% L-glutamic acids for 24 h. After that, the cells were washed with PBS and incubated in 100 μ L of FBS-free medium, which were treated with polyplexes (prepared as describe earlier) to a final concentration of 1 μ g of DNA/well. After 4 h, the treated medium was exchanged for fully supplemented medium (DMEM supplemented with 10% FBS and 1% L-glutamic acids) and incubated for further 24 h. The metabolic activity of cells was determined by adding 25 μ L of MTT reagent (5 mg/mL in PBS) per well. The cells were incubated for 3 h after adding the reagent and washed with PBS, and then 150 μ L of dimethyl sulfoxide was added before reading the absorbance at 570 nm using cells treated with FBS-free medium and Triton 0.2% as a positive control and a negative control, respectively. The percentage of metabolic activity was calculated using the following equation:

$$\text{Metabolic activity (\%)} = S - T/C - T * 100$$

where *S* is the absorbance obtained with the tested samples, *T* is the absorbance observed with Triton, and *C* is the absorbance observed with the untreated cells.

In vitro transfection study

A549 or H1299 cells were seeded into a 24-well plate at a density of 5 \times 10⁴ cell/well and incubated in 500 μ L of fully supplemented medium for 24 h. Then, the cells were washed with PBS, covered with 500 μ L of Opti-MEM (Reduced Serum Media from Thermo Fisher) and

treated with gWiz-Luc polyplexes at a concentration of 1 μg of DNA/well (in the case of transfection with chloroquine, a final concentration of 100 μM was used). After 4 h, the transfection medium was replaced with fully supplemented medium, and the cells were incubated for further 24 h. After this time, the cells were washed with PBS, and the expression of luciferase was detected using a luciferase assay kit.

Cellular uptake and LysoTracker studies

Polyplexes were prepared using FITC-labelled polymers and Cy3-labelled plasmids to study the cellular uptake. For confocal microscopy, cells were seeded into eight-well chamber slides at a seeding density of 2×10^4 in 300 μL fully supplemented medium. After 24 h, the cells were washed with PBS, covered with 300 μL of Opti-MEM, and treated with the labelled polyplexes to a final concentration of 0.6 μg of DNA/well for 4 h. Then, the cells were washed with PBS three times, fixed with 4% paraformaldehyde for 15 min, stained with DRAQ5 (20 μM in PBS for 5 min), and then covered with mounting medium. In case of LysoTracker experiments, the washed cells were treated with LysoTracker Green DND-26 (100 nM) for 10 min and stained with Hoechst (1 $\mu\text{g}/\text{mL}$) for further 10 min, and then the cells were washed and imaged directly. For flow cytometry, the cells were prepared in conditions similar to those in the transfection experiments. After incubation of cells with labelled polyplexes for 4 h, the cells were washed with PBS three times and then detached from the plates using 500 μL of Accutase solution for 15 min

at 37°C. The cells were collected in FACS tubes and measured directly using Astrios flow cytometer (from BECKMAN COULTER, USA).

Results and Discussion

A small library of thermally polymerised hyperbranched polymers was constructed and characterised. The prepared *hb*-polyK and *hb*-polyKH with three different molar ratios of histidine were categorised into two groups (groups A and B) according to their experimentally determined molecular masses, as reported in Table 1.

Synthesis and characterisation of hyperbranched polymers

Hyperbranched polymers were prepared via thermal polycondensation of amino acids (step-growth polymerisation) in a method adapted with minor modifications from that of Scholl et al. (2007b). Lysine-HCl alone or in the presence of histidine (at different molar ratios) was neutralised using KOH to liberate the free amino acid for polymerisation and leaving metal salt (KCl) as a by-product (Scheme 1). The reactions were carried out using equimolar amounts of lysine-HCl and KOH with, in case of *hb*-polyKH, 1, 2, or 4 mol of histidine per 10 mol of lysine-HCl. A small quantity of water (20-30 mL) was added to facilitate the neutralisation of lysine-HCl, as described by Kadlecova et al. (2012a). The reaction mixtures were then heated to 150°C under a nitrogen stream with mechanical stirring. These conditions removed water vapour to minimise hydrolysis and to force conversion to higher

Table 1. Characteristics of thermally polymerised hyperbranched polymers.

	K : H ratio ^{†1}	M_n (kDa) ^{†2}	M_w (kDa) ^{†2}	PDI (Đ)	DB	ANB	T_g (°C)	Buffer capacity ^{†3} (%)	μmol of amine ^{†4}
Group A									
<i>hb</i> -polyK-13kDa	—	13.4	22.7	1.7	0.34	0.24	56.6	35.2	5.3
<i>hb</i> -polyKH ₁ -19kDa	10:1	19.6	29.5	1.5	0.41	0.34	81.5	39.7	4.4
<i>hb</i> -polyKH ₂ -18kDa	10:2	18.1	25.3	1.4	0.46	0.39	98.9	44.0	4.0
<i>hb</i> -polyKH ₄ -16kDa	10:4	16.0	27.9	1.7	0.49	0.40	107.5	43.6	4.3
Group B									
<i>hb</i> -polyK-33kDa	—	33.6	58.8	1.7	0.39	0.27	65.3	37.4	5.3
<i>hb</i> -polyKH ₁ -44kDa	10:1	44.7	87.7	1.9	0.40	0.32	90.1	41.7	3.9
<i>hb</i> -polyKH ₂ -34kDa	10:2	34.5	62.8	1.8	0.40	0.32	108.6	43.9	3.6
<i>hb</i> -polyKH ₄ -33kDa	10:4	33.2	51.7	1.5	0.43	0.35	112.6	44.5	3.8

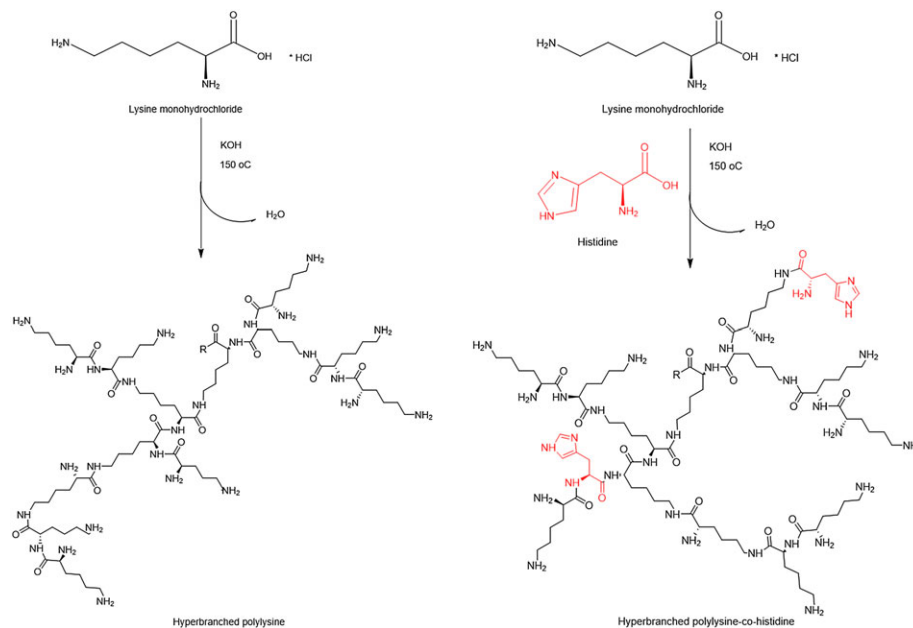
ANB, average number of branches; DB, degree of branching.

^{†1}Molar ratios of lysine to histidine.

^{†2}Multangle laser light scattering detector gel permeation chromatography molecular masses.

^{†3}Buffer capacity at pH range of 5-7.

^{†4} μmol of amine/mg of polymers (fluorescamine assay).



Scheme 1. Thermal polycondensation for synthesis of hyperbranched polymers.

molecular mass. The polymerisations were also carried out under an inert atmosphere to minimise oxidation, degradation, and decarboxylation (Kricheldorf, 1992). As step-growth polymerisation is time dependent and based on functional group conversion; the molecular mass was controlled by conducting the reactions for 24 and 48 h to construct two sets of polymers, denoted as polymer groups A and B (Table 1). Reactions that proceeded for a longer time (>48 h) produced cross-linked gels, most likely due to deamination reactions and formation of secondary amine linkages as reported in the synthesis of nylon-type polyamides (Yang, 2006). The characterisation data (FT-IR, $^1\text{H-NMR}$, and $^{13}\text{C-NMR}$) were in agreement with those previously reported in the literature for similar PLL materials (Scholl et al., 2007b, Kadlecova et al., 2013). NMR data of the histidine-containing copolymers displayed the characteristic signals of the imidazole ring, and integration of these peaks enabled the amount of incorporated histidine in each polymer to be determined (Figs. S1-S7). According to Scholl et al. (2007b), who compared the $^1\text{H-NMR}$ spectra of *hb-polyK* with those of poly(α -lysine), poly(ϵ -lysine), and dendritic PLL, four different resonances of α -CH protons can be recognised in the spectra of *hb-polyK* corresponding to its different structural units (dendritic, terminal, α -linear, and ϵ -linear). The $^1\text{H-NMR}$ spectra of the *hb-polyK* prepared in this study showed excellent similarity with those reported by Scholl et al. (2007b)

and Kadlecova et al. (2012a). In addition, the spectra of the histidinylated polymers displayed the same peaks, suggesting that the resonances at 4.13, 3.85, 3.33, and 3.23 ppm corresponded to the α -CH protons of dendritic, α -linear, terminal, and ϵ -linear units, respectively. This was confirmed by heteronuclear single quantum correlation spectra (Fig. S8 and S9), which clearly showed that the protons of these peaks were connected to the α -C in both polymers (*hb-polyK* and *hb-polyKH*). By integrating these peaks, the structural parameters were calculated (Table 1). The DB values were within the reported range for hyperbranched polymers and less than 0.5 (the value expected for hyperbranched polymers obtained by the polymerisation of an AB₂ monomer with B functionalities that have equal reactivity) (Scholl et al., 2009). This reflected the fact that the ϵ -amine is more nucleophilic than the α -amine in lysine. Interestingly, the DB values of histidinylated polymers were higher than those of *hb-polyK*, where the DB increasing from 0.34 for *hb-polyK-13kDa* to 0.46 and 0.49 for *hb-polyKH₂-18kDa* and *hb-polyKH₄-16kDa*, respectively. The same trend can be seen with polymers of higher molecular mass (group B, Table 1), indicating that the addition of histidine modulated the reaction pathways to produce increasingly dendritic architectures. We attribute this to the replacement of the most reactive amine of lysine (ϵ -amine) by histidine, thus directing the polymerisation towards the less reactive α -amine of lysine and

the imidazole amines in histidine. This conclusion can be supported by the work of Scholl et al. (2007a) who reported the feasibility of modulating the structure of *hb*-polyK by the temporal protection of the lysine ϵ -amine during polymerisation.

In order to develop a better understanding of the effect of histidine on the structure of the hyperbranched polymers, the thermal and rheological behaviours of the polymers were investigated. The DSC data (Fig. 1A) revealed a significant increase in the glass transition temperature (T_g) with increasing histidine content in the polymers, where the T_g values changed from 56.6°C for *hb*-polyK-13kDa to 81.5°C, 98.9°C, and 107.5°C for *hb*-polyKH₁-19kDa, *hb*-polyKH₂-18kDa, and *hb*-polyKH₄-16kDa, respectively. Several factors affect the value of T_g , but the flexibility of polymer chains is cited as the most important (Chanda, 2000). The increased T_g values of increasingly histidinylated polymers may have been a consequence of more rigid materials with restricted movements of their chains. This may be explained by the bulkiness of the imidazole ring of histidine as a side group (Kunal et al., 2008; Dudowicz et al., 2005) and by the effect of histidine on the DB of the polymers. For polymers with a low number of branches, an increase of branches relative to the overall mass numbers of branches, an increase in side groups can stiffen the material and restrict chain mobility,

thereby raising T_g (Chanda, 2000). The increase in T_g for the histidinylated polymers was therefore suggestive of high branching.

Regarding the rheological behaviour, all the polymers, compared with linear polymers with extended and entangled chains, exhibited Newtonian flow (Fig. 1B) as expected for dendritic and hyperbranched polymers with globular structures and reduced chain entanglement (Le et al., 2009). Also, polymers with higher histidine content were slightly more viscous than were *hb*-polyK, perhaps owing to interchain π - π interactions of the imidazole rings on these polymers.

In order to illustrate the effect of histidine on the buffer capacity of the hyperbranched polymers, acid-base titrations were performed. The results indicated that the percentage of ionisable amines, under pH values 5-7, is likely to be encountered in endosomal compartments during cellular processing, scaled with histidine content. The buffer capacity increased from 35.2% for *hb*-polyK-13kDa to 43.6% for *hb*-polyKH₄-16kDa; the same trend was obtained for polymers of higher molecular mass (Table 1). The effect of histidine can be clearly seen in the titration curves (Fig. 1C), where the histidinylated polymers displayed a marked buffering region at pH values between 4 and 6 in contrast to *hb*-polyK-13kDa over the same pH range. The averaged pK_a of the imidazole amines in the polymers was 5.1 as measured by ¹H-NMR (Fig. S10), which

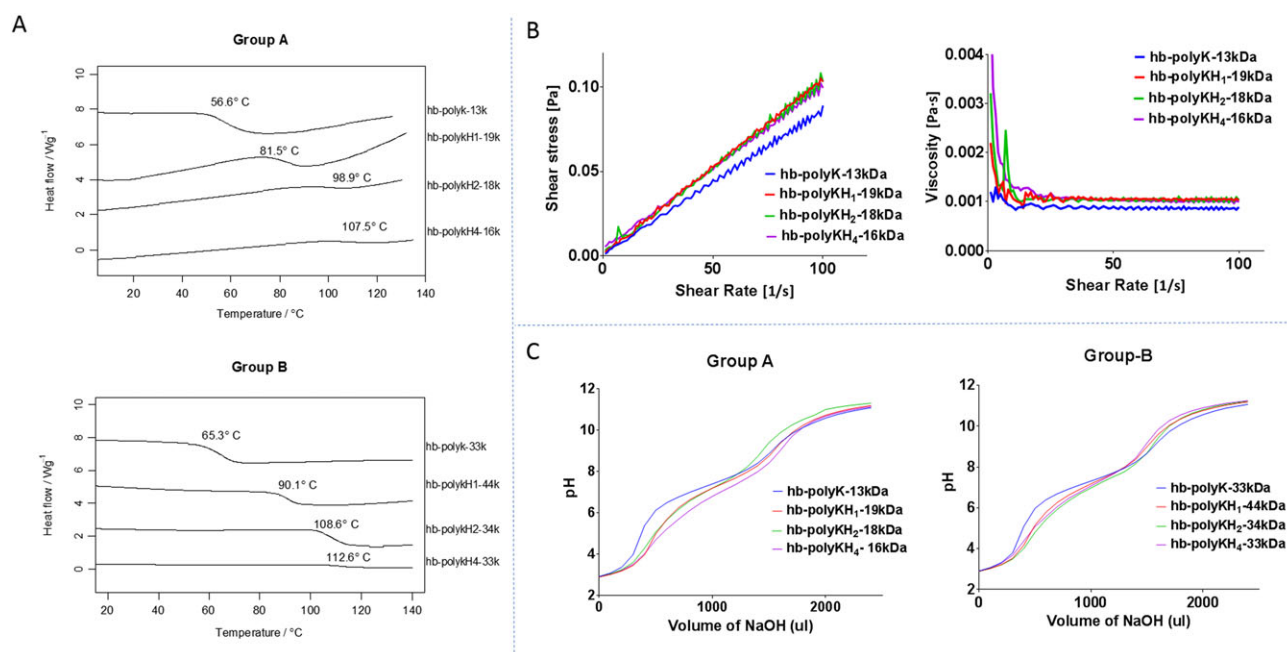


Figure 1. (A) Glass transition temperature of hyperbranched polymers in groups A and B. (B) The rheological behaviour of hyperbranched polymers, the shear rate versus the shear stress, and viscosity. (C) pH-titration curves of hyperbranched polymers in groups A and B.

explains the behaviour of histidinylated polymers at this pH range. The different pK_a of imidazole amines in the hyperbranched copolymer in comparison with that of free histidine ($pK_a = 6$) provided an indication of the distribution of histidine residues in the overall polymer structure. Reduced basicity (i.e., low pK_a) amines were likely to have arisen from closely proximal imidazole rings, either from “blocky” regions in the polymer or from less accessible histidines in the “core” of the branched structure. It was also apparent from the titration curves that the polymers also showed a good buffer capacity at pH 7-8, owing to the effect of α -amino groups (deriving from ϵ -amine-linked polyamide units).

Preparation and characterisation of polyplexes

As the complexation of nucleic acids with polycations is mainly defined by electrostatic interactions, it is important to know, with high precision, the number of amine groups in the polymers. Fluorescamine selectively reacts with primary amines to give a highly fluorescent fluorophore (Udenfriend et al., 1972) and so was utilised to quantify reactive amines in the synthesised polymers (Table 1), thus allowing accurate calculation of N/P ratios for the formation of polyplexes.

Representative AFM images and dynamic light scattering (DLS) data of polyplexes (Fig. 2A, B) prepared in a low ionic strength buffer indicated that the polymers are capable of condensing DNA into polyplexes of sub-200 nm in radii, even at relatively low N/P ratios of ~ 3 , apart from highly histidinylated and branched polyKH₄-16kDa. The AFM images showed that the polymers formed compact and spherical polyplexes with diameters of sub-200 nm and average size distribution smaller than those reported by DLS (Fig. S11A). The differences between AFM and DLS measurements are probably due to the difference in the origin of the presented data, where the presented data of DLS represent the intensity distribution, while the AFM values are more likely reflecting the number distribution of polyplexes. Also, unlike the hydrated and freely interacting polyplexes in DLS measurements, it is expected that the AFM measurements give smaller sizes where the polyplexes are dried and confined to the surface of the mica.

Notably, the histidinylated polymers generally formed larger complexes than did the *hb*-polyK polymers (Fig. 2B), and their condensation behaviour was composition dependent, as shown most clearly in gel electrophoresis. The appearance of free DNA bands at

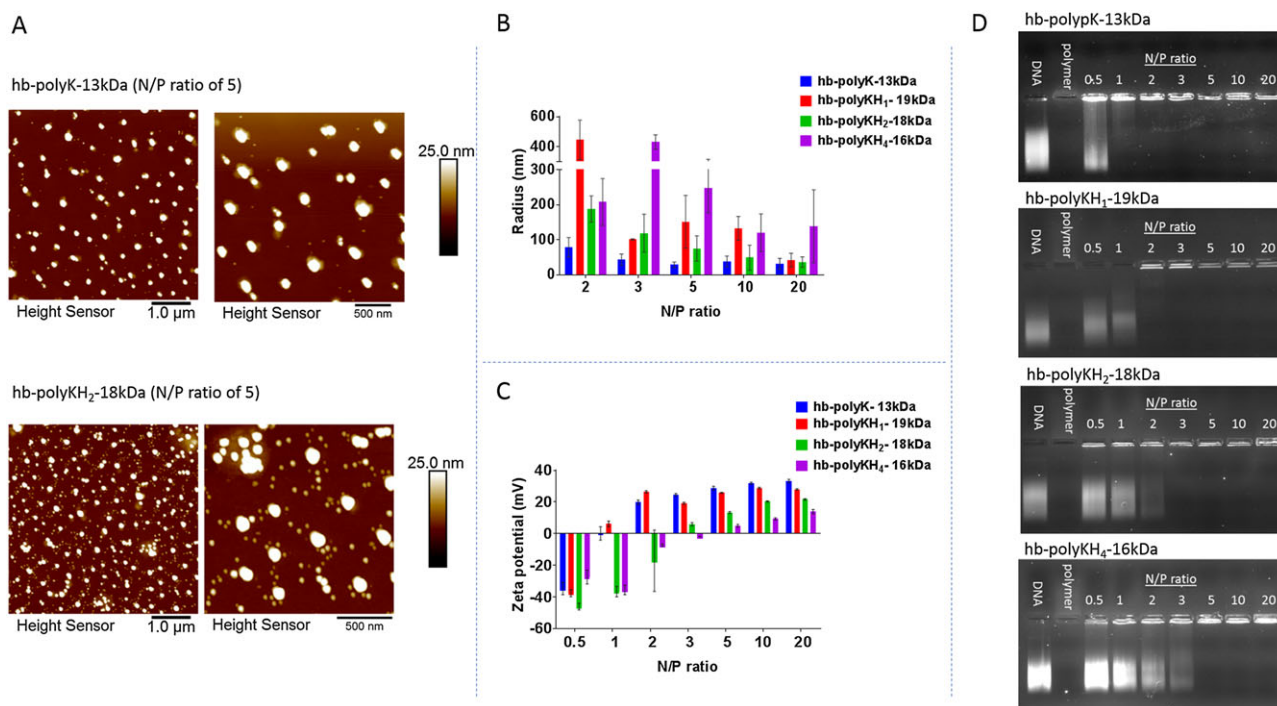


Figure 2. (A) Atomic force microscopy images (N/P ratio of 5). (B) Average dynamic light scattering radii of polyplexes prepared in HEPES buffer (10 mM, pH 7.4). (C) Average zeta potential values for polyplexes prepared at different N/P ratios (in 10 mM HEPES, pH 7.4) using polymers of group A. (D) Agarose gel electrophoresis of hyperbranched polymers/DNA polyplexes prepared in phosphate-buffered saline, pH 7.4 at different N/P ratios.

higher N/P ratios as histidine content increased is apparent from Figure 2D, and in the composition dependence of average zeta potential values at all N/P ratios (Fig. 2C). For the particular example of a highly histidinylated polymer, that is, *hb*-polyKH₄-16kDa, a higher N/P ratio was required for efficient DNA condensation. In addition, the change in zeta potential from negative to positive values for the *hb*-polyKH₄ complexes occurred at higher N/P ratio. Thus the overall average zeta potential values were lower for this polymer when complexed with DNA compared with other complexes (Fig. 2C), and, consequently, the *hb*-polyKH₄ complexes were of larger particle size (Fig. 2B) and with a greater tendency to aggregate. It is also noticeable that introduction of histidine in *hb*-polyKH copolymers resulted in higher levels of ethidium bromide intercalation at the plateau (N/P ratios > 3 in Figure S12), indicating a reduced DNA condensation, relative to the *hb*-polyK homopolymer. Such behaviour could be a consequence of the stiffer nature of *hb*-polyKH molecules, as seen in their increased *T*_g values (Fig. 1A).

Taken together, the data in Figure 2 illustrate that all polymers were capable of complexing DNA and achieved maximum DNA complexation and condensation close to neutralisation point (zeta potential reversal N/P ratio). Any further addition of polymers (N/P ratios of 5, 10, and 20) affected the surface charges of the polyplexes but did not markedly alter particle size.

For the higher molecular mass polymers (group B), gel electrophoresis (Fig. S12) indicated a complete retardation of DNA at N/P ratio of 2, and polyplexes were formed with higher positive surface charge (even for high histidine content *hb*-polyKH₄-33kDa polymer) than were those with the lower molecular mass polycations. The longer-chain-length polymers also produced smaller complexes (~100 nm in radii) than did the lower molecular mass analogies at equal N : P ratio.

In the higher ionic strength buffer, all the polyplexes tended to aggregate, an effect that was especially pronounced for low-molecular-mass polymers (Fig. S11), reflecting the fact that their colloidal stability is dependent on electrostatic repulsion, in the absence of steric stabilisation components.

Biological evaluation of polyplexes

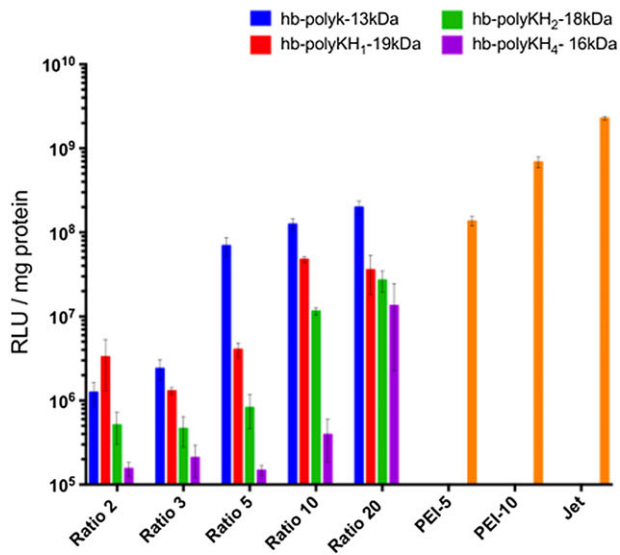
In prior literature, it has been widely reported that polycations can be toxic and that their toxicity is a function of parameters including molecular mass, charge density, structure and conformational flexibility,

concentration, and incubation time (Fischer et al., 2003, Hall et al., 2017). Thus, in order to check the cytocompatibility of the hyperbranched materials, the effects of the polymers and their complexes on the metabolic activity of A549 cells were investigated using MTT assays. The results (Fig. S13) indicated that the polyplexes of low-molar-mass polymers (group A) were well tolerated by the cells, even when applied at concentrations higher (approximately four times) than the concentrations used in the transfection study. Toxicity became apparent with polymers of higher histidine content and higher molecular mass, *hb*-polyKH₂-34kDa and *hb*-polyKH₄-33kDa, where a reduction in metabolic activity (>80%) was detected at N/P ratios > 5. Nevertheless, the cell viability for all polymers at high N/P ratio of 20 was higher than for corresponding PEI complexes.

In order to evaluate the capability of polymers to act as delivery agents for nucleic acids, A549 and H1299 cell lines were selected (as representative cancer cells) for transfection with a luciferase reporter plasmid DNA (gWiZ-Luc), as reported in Figure 3. In A549 cells, the best luciferase activity was detected for polyplexes of lysine-only *hb*-polyK-13kDa polymer, which was comparable with that obtained by PEI (N/P of 5), under the conditions of the experiment. For the *hb*-polyKH of group A (Fig. 3A), the results revealed that the transfection efficiency increased as N/P ratio was increased, but, importantly, transfection decreased with an increase in histidine content of the polymers, for all N/P ratios applied. In H1299 cells (Fig. 3B), a similar trend of transfection can be observed for polyplexes in group A at low N/P ratios. Significantly, however, the transfection of highly histidinylated polymers (*hb*-polyKH₂-18kDa and *hb*-polyKH₄-16kDa) was enhanced at high N/P ratios and was found to be better than that of *hb*-polyK-13kDa at N/P ratio of 20.

Also, it should be noted that the transfection efficiencies of the high-molecular-mass polymers (group B) were not appreciably improved at high N/P ratios in both cell lines (Fig. S14). This behaviour may have been due to the formation of more stable poly-electrolyte complexes by the higher molecular mass polymers, leading to poor intracellular unpackaging and DNA release. This interpretation was further supported by particle size measurements, which showed that at high N/P ratios of high-molecular-mass polymers, smaller and thus more tightly packed polyplexes were mostly formed. The higher stability of the complexes was also demonstrated by heparin competition assays as shown in Figure S15.

(A) A549 cells



(B) H1299 cells

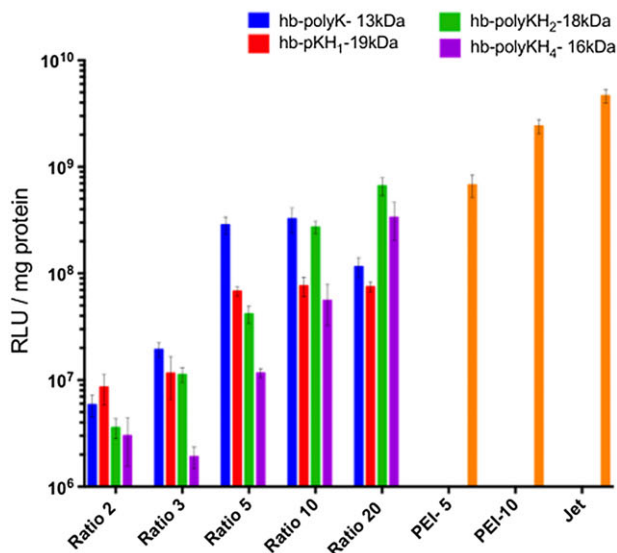


Figure 3. Luciferase activity of (A) A549 and (B) H1299 cells treated with polyplexes prepared with polymers in group A, in comparison with PEI (N/P ratios of 5 and 10) and jetPRIME® as positive controls. PEI, polyethylenimine; RLU, relative light units.

Considering the previously reported increase in transfection efficiencies of polymers on introduction of histidine to PLL (Soliman et al., 2012, Nasanit et al., 2008), a comparison was made on the basis of the level of cellular uptake of the *hb-polyK* (lysine-only) and *hb-polyKH₂* (histidine-containing) complexes. Confocal microscopy images (Fig. 4A) showed rapid accumulation of polyplexes inside the cells with apparent association between regions of dual fluorescence and

the nuclei of the cells. Flow cytometry results (Fig 4B) showed that the lysine-only polymers were taken up more efficiently than were the histidinylated polymers in A549 cells, while in H1299 cell line, the differences were insignificant. The internalisation of the polyplexes could be correlated with an increased zeta potential of the lysine-only polyplexes (Fig. 2C) and potentially increased association of more positively charged polyplexes with the cell surface, as reported earlier (Bannunah et al., 2014, He et al., 2010). The manifest difference in cellular internalisation of *hb-polyKH₂-18kDa*, and the corresponding lysine-only *hb-polyK-13kDa* complexes in A549, was thus attributable to the effects of the histidine residues. The factors by which histidine residues affected internalisation may have been a combination of decreased charge at pH 7.4, greater polymer stiffness, and also increased particle size. In turn, the lower transfection levels seen for *hb-polyKH* polymers were likely related to the reduced cellular internalisation of their polyplexes. However, the specific individual factors and their combinations are not easy to correlate directly with the significant drop in transfection associated with the increase of histidine content in the polymers. Also, no direct link could be established with the marked increase of transfection in H1299 cells and as a function of N/P ratios where, apart from N/P ratio of 5 in A459, the uptake of each polymer showed insignificant variation between different N/P ratios, which indicated that the intercellular trafficking of the polyplexes was affected significantly as well.

Accordingly, the endosomal escape of the *hb-polyK-13kDa* and *hb-polyKH₂-18kDa* polyplexes was investigated through LysoTracker experiments as shown in Figure 5A. The Pearson coefficients (ρ), calculated for the confocal images of LysoTracker, indicated that there was a higher correlation ($\rho = 0.49$) and tendency of colocalisation between the *hb-polyKH₂-18kDa* polyplexes and the endosomal/lysosomal pathway of the cells in comparison with the *hb-polyK-13kDa* polyplexes ($\rho = 0.33$). To obtain further insight, *hb-polyK-13kDa* and *hb-polyKH₂-18kDa* polyplexes of N/P ratio of 10 were selected for transfection experiments, which included the endosomolytic agent, chloroquine. The results, shown in Figure 5B, indicated that the chloroquine did not change the transfection of *hb-polyK-13kDa* in either cell line. These data were in accord with those of Kadlecova et al. (2013) who found that bafilomycin A, an ATPase inhibitor that decreases acidification of early endosomes, inhibited

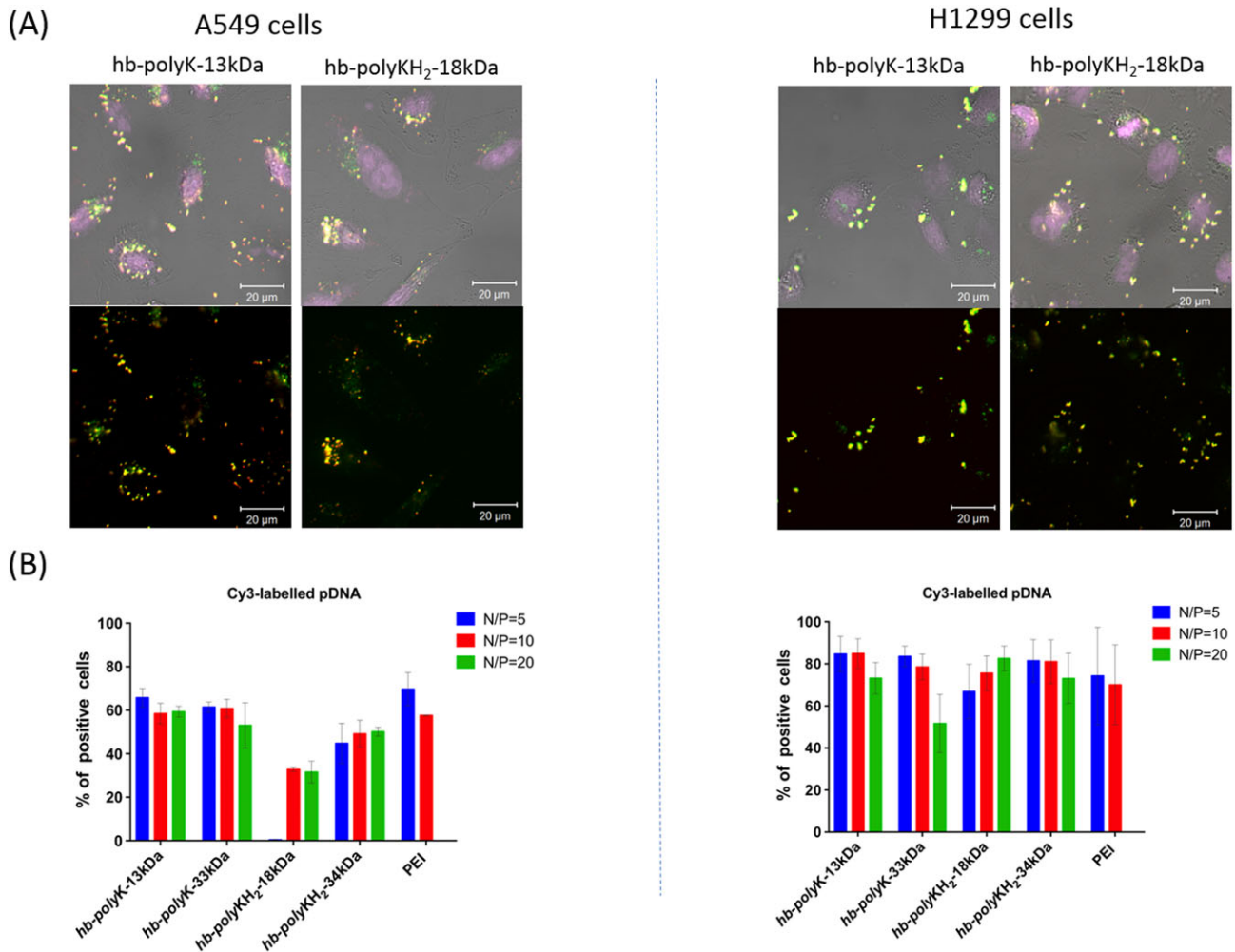


Figure 4. Endocytosis of *hb-polyK* and histidine-containing *hb-polyKH₂* complexes in A549 and H1299 cells. (A) Confocal images and (B) quantification of fluorescent species by flow cytometry. Areas in green are FITC-labelled polymers, regions in yellow are assigned to overlaid Cy3-labelled plasmid (true colour = red) and FITC-labelled polymers, and areas in purple correspond to DRAQ5 stained nuclei. FITC, fluorescein isothiocyanate.

transfection with *hb-polyK* whereas chloroquine did not. Interestingly, the transfection of *hb-polyKH₂-18kDa* was significantly increased to a level comparable with that of *hb-polyK-13kDa* in H1299 cells, but in A549 cells, the effect of chloroquine was insignificant. Chloroquine can be trapped in the acidifying endosomes leading to the osmotic swelling and membrane disruption of endosomes (Cheng et al., 2006, Zhang and Wagner, 2017). Thus, the results suggest that the effect of buffer capacity (proton sponge) in the polymers had a notable impact on the capacity for endosomal escape in H1299 but not in A549 cells.

The mechanism of endosomal escape for these cationic polymers was likely a synergistic effect of direct endosome membrane interaction and destabilisation, and proton sponge behaviour due to buffering capacity. This synergistic effect could explain the differing

transfections of hyperbranched polymers in A549 and H1299 cell lines. The incorporation of histidine may have led to a reduced capability, or loss of preferred confirmation, of the histidinylated polymers to interact with endosome membranes. This in turn could have led to reduced membrane destabilisation by the histidinylated polymers, and membrane-lysis activity more via buffer capacity and proton sponge behaviour. Given that A549 cells have been reported to display more stable membranes than did H1299 (Tedja et al., 2011, Lieber et al., 1976), the impact of reduced membrane destabilisation would have been more significant in the transfection of A549 cells. This interpretation is supported by the lower transfection activity of histidinylated polymers, even at high N/P ratios, in comparison with that of *hb-polyK*. The results of lactate dehydrogenase assays (Fig. S16) showed that *hb-polyK-*

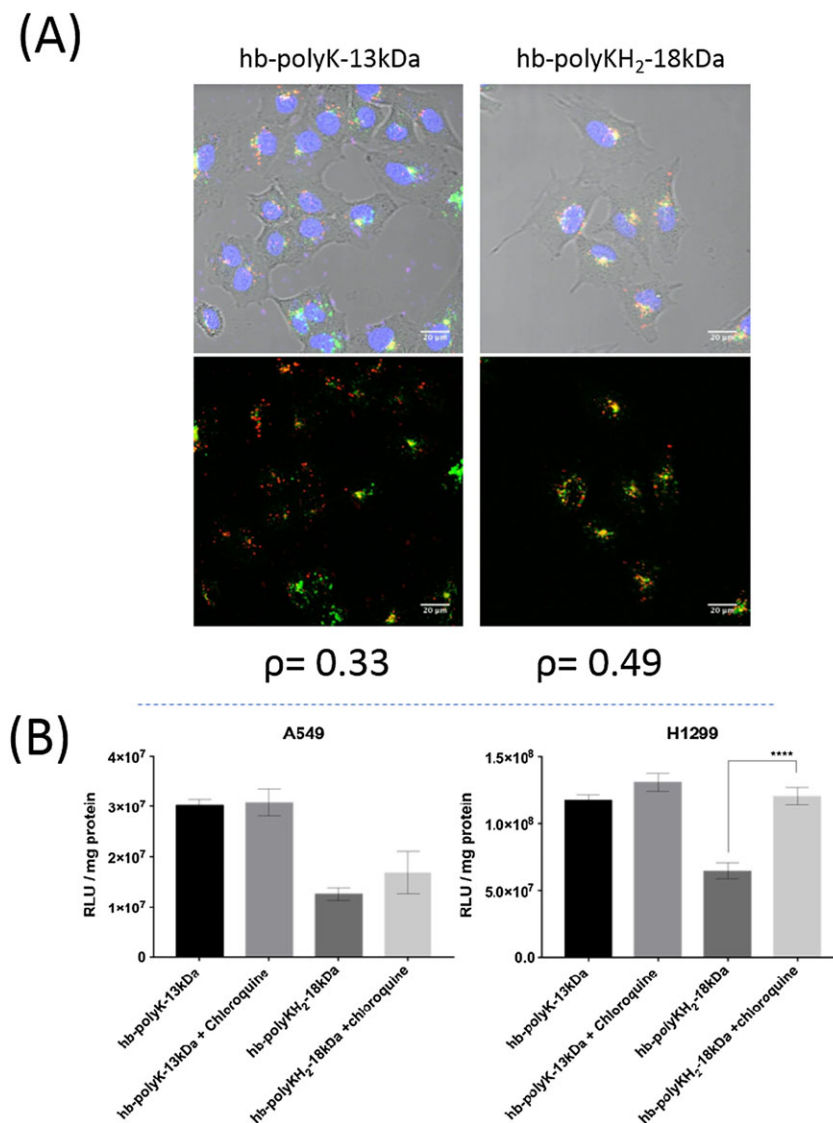


Figure 5. (A) Confocal images of LysoTracker experiment and (B) % luciferase expression of cells treated with chloroquine. Areas in green are LysoTracker, regions in red are Cy3-labelled plasmid of polyplexes, and areas in blue correspond to Hoechst-stained nuclei. RLU, relative light units.

13kDa was able to permeabilise the membranes in H1299 cells at much lower N/P ratio than in A549 cells, in comparison with *hb-polyKH₂-18kDa*, providing additional evidence for the membrane activity hypothesis.

As reported in the pH-titration profiles (Fig. 1C), the overall buffer capacity of the polymers increased with increasing histidine content. However, the average pKa of the imidazole amines in these polymers (pKa = 5.1, Fig. S10) was at the lower end of the predicted endosomal pH range, which may have limited their proton sponge capabilities. In prior work, Iacobucci et al. (2012) used a histidine-rich peptide of low pKa and found delays in the endosomal escape of peptide-nucleic acid complexes with less efficient

transfection. Also, Roufai and Midoux (2001) found that the acetylation of α -amines in a post-polymerisation histidinylated PLL produced a shift in the pKa of imidazole rings to a lower value. This in turn led to low transfection, attributed to the role of early imidazole ionisation in endosomal escape via direct interaction and destabilisation of the endosomal membrane.

The reduced transfection efficiencies were most probably also a consequence of polymer architecture per se. Kadlecova et al. (2013) found that hyperbranched PLL was a superior transfection agent than was linear and dendritic PLL. The introduction of histidine units within the polymer afforded more

branched/dendritic polymers, and these were found to be more compact and rigid in structure than were *hb*-polyK. Subsequently, the *hb*-polyKH polymers were less efficient in condensing DNA into discrete and stable polyplexes, which may have negatively impacted on the extent of their association with, and internalisation by, cells. In addition, the potential for blockiness in the histidine-containing polymers as a result of their mode of synthesis may have altered the local pKa values of the imidazole rings such that they were less able to bind effectively to DNA and also to buffer endosomal pH such that the polyplexes could escape intracellular digestive pathways. The former factor would reduce polyplex charge and stability, leading to reduced endocytosis, while the reduced buffering capacity would have impaired their ability to disrupt intracellular barriers such as endosomal and nuclear membranes, again leading to reduced transfection.

Taken together, the results indicated that, for A549 cell line at least, the incorporation of histidine within *hb*-polyK enhanced buffering capacity as expected but did not increase gene delivery efficiency. However, the data also indicate that the materials' synthesis route, and the corresponding architecture obtained, altered the behaviour of the polymers in ways that were more subtle than via a simple change in protonation state at physiologically relevant pH values. NMR and T_g data, as well as rheology measurements, indicated greater stiffness in the histidine polymers and, possibly also increased blockiness, leading to lowered pKa and reduced buffer capacity at endosomal pH. The blockiness and stiffness were a consequence of the thermal polycondensation route, whereby branching took place more readily with the histidine polymers, and from which more linear sections of poly(lysine) grew. The position histidine residues as branch points effectively placed them as less accessible "core regions" of the polymer, and with less capacity to interact with nucleic acids. Thus, the critical findings of this study are that it is not just incorporation of histidine units in a polymer but also how and where these units are introduced, which are central to gene delivery function. Control of monomer sequence and chain structure is clearly required to balance parameters such as conformational flexibility, buffering capacity and strength of carrier polymer interactions with nucleic acids. Natural poly(amino acids) have been evolved to be conformable enough to condense DNA efficiently, to be stable in polyelectrolyte complexes to traverse

cell membranes, and to trigger mechanisms that can unpackage nucleic acid cargoes in the desired cellular location. The data from our study have provided valuable insight into the design criteria for polymers, which can effectively act as DNA delivery agents in vitro but also have indicated potential constraints in trying to simplify synthetic procedures towards highly complex materials while retaining the ability of those materials to function in their intended biological application.

Conclusions

In summary, *hb*-polyKH polymers were prepared via a simple thermal polycondensation of the parent amino acids and compared with *hb*-polyKs, which were synthesised by known routes to well-established structures. The effects of histidine incorporation on the architectures of the polymers and on their gene delivery efficiency were investigated. The results revealed that histidine residues modulated the structure of polymers by competing with the more reactive ϵ -amine of lysines, thus directing the polymerisation towards the α -amine of the monomers. As a consequence, more branched, dendritic polymers were prepared, with increased rigidity, as indicated by the DB and T_g values. The histidine-containing polymers, in comparison with lysine-only polymers, afforded polyplexes with lower surface charges and a higher tendency to aggregate. Furthermore, the results revealed that the histidine incorporation has a significant impact on the transfection of the polyplexes and their intracellular behaviour. Although the histidine residues enhanced the buffer capacity, they affected the charge and flexibility of the histidinylated polymers and thus their ability to interact and destabilise the biological membranes, which in turn reduced the cellular internalisation and the level of transfection, in particular in A549 cells. The results together indicate that co-monomer content can affect multiple properties in a poly(amino acid) prepared by thermal polycondensation, and that co-monomer placement and sequence can markedly affect gene delivery importance even in polymers synthesised by these simple routes.

Acknowledgments

This work was funded by the Engineering and Physical Sciences Research Council (grant EP/H005625/1), the Royal Society, via a Wolfson Research Merit Award

(WM150086) to CA and the Higher Committee for Education Development in Iraq (scholarship to AA).

Data Access Statement

All raw data created during this research are openly available from the corresponding author (cameron.alexander@nottingham.ac.uk) and at the University of Nottingham Research Data Management Repository (<https://rdmc.nottingham.ac.uk/>), and all analysed data supporting this study are provided as Supporting Information accompanying this paper.

Conflict of Interest

None declared.

REFERENCES

- Ainallem, M. L., Carnerup, A. M., Janiak, J., Alfredsson, V., Nylander, T., and Schillen, K. **2009**. Condensing DNA with poly(amido amine) dendrimers of different generations: means of controlling aggregate morphology. *Soft Matter* 5:2310-2320.
- Altnoglu, S. A., Wang, M., Li, K. Q., Li, Y., and Xu, Q. **2016**. Intracellular delivery of the PTEN protein using cationic lipidoids for cancer therapy. *Biomater. Sci.* 4:1773-1780.
- Bannunah, A. M., Vllasaliu, D., Lord, J., and Stolnik, S. **2014**. Mechanisms of nanoparticle internalization and transport across an intestinal epithelial cell model: effect of size and surface charge. *Mol. Pharm.* 11:4363-4373.
- Bansal, R., Tayal, S., Gupta, K. C., and Kumar, P. **2015**. Bioreducible polyethylenimine nanoparticles for the efficient delivery of nucleic acids. *Org. Biomol. Chem.* 13:3128-3135.
- Blum, A. P., Kammeyer, J. K., and Gianneschi, N. C. **2016**. Activating peptides for cellular uptake via polymerization into high density brushes. *Chem. Sci.* 7:989-994.
- Chanda, M. **2000**. *Advanced Polymer Chemistry: A Problem Solving Guide*. Marcel Dekker, New York.
- Chen, X. Y., Lai, H. W., Xiao, C. S., Tian, H. Y., Chen, X. S., Tao, Y. H., and Wang, X. H. **2014**. New bio-renewable polyester with rich side amino groups from L-lysine via controlled ring-opening polymerization. *Polym. Chem.* 5:6495-6502.
- Cheng, J. J., Zeidan, R., Mishra, S., Liu, A., Pun, S. H., Kulkarni, R. P., Jensen, G. S., Bellocq, N. C., and Davis, M. E. **2006**. Structure-function correlation of chloroquine and analogues as transgene expression enhancers in nonviral gene delivery. *J. Med. Chem.* 49:6522-6531.
- Cho, S. K., Dang, C., Wang, X., Ragan, R., and Kwon, Y. J. **2015**. Mixing-sequence-dependent nucleic acid complexation and gene transfer efficiency by polyethylenimine. *Biomater. Sci.* 3:1124-1133.
- De Smedt, S. C., Demeester, J., and Hennink, W. E. **2000**. Cationic polymer based gene delivery systems. *Pharm. Res.* 17:113-126.
- Dudowicz, J., Freed, K. F., and Douglas, J. F. **2005**. The glass transition temperature of polymer melts. *J Phys Chem B* 109:21285-21292.
- Dufes, C., Uchegbu, I. F., and Schatzlein, A. G. **2005**. Dendrimers in gene delivery. *Adv. Drug Deliv. Rev.* 57:2177-2202.
- Fischer, D., Li, Y., Ahlemeyer, B., Krieglstein, J., and Kissel, T. **2003**. In vitro cytotoxicity testing of polycations: influence of polymer structure on cell viability and hemolysis. *Biomaterials* 24:1121-1131.
- Godbey, W. T., Wu, K. K., and Mikos, A. G. **2001**. Poly(ethylenimine)-mediated gene delivery affects endothelial cell function and viability. *Biomaterials* 22:471-480.
- Hall, A., Lachelt, U., Bartek, J., Wagner, E., and Moghimi, S. M. **2017**. Polyplex evolution: understanding biology, optimizing performance. *Mol. Ther.* 25:1476-1490.
- Hardy, J. G., Love, C. S., Gabrielson, N. P., Pack, D. W., and Smith, D. K. **2009**. Synergistic effects on gene delivery-co-formulation of small disulfide-linked dendritic polycations with Lipofectamine 2000™. *Org. Biomol. Chem.* 7:789-793.
- Hawker, C. J., Lee, R., and Frechet, J. M. J. **1991**. One-step synthesis of hyperbranched dendritic polyesters. *J. Am. Chem. Soc.* 113:4583-4588.
- He, C., Hu, Y., Yin, L., Tang, C., and Yin, C. **2010**. Effects of particle size and surface charge on cellular uptake and biodistribution of polymeric nanoparticles. *Biomaterials* 31:3657-3666.
- Hölter, D., Burgath, A., and Frey, H. **1997**. Degree of branching in hyperbranched polymers. *Acta Polym.* 48:30-35.
- Hurley, C. A., Wong, J. B., Ho, J., Writer, M., Irvine, S. A., Lawrence, M. J., Hart, S. L., Tabor, A. B., and Hailes, H. C. **2008**. Mono- and dicationic short PEG and methylene dioxyalkylglycerols for use in synthetic gene delivery systems. *Org. Biomol. Chem.* 6:2554-2559.
- Iacobucci, V., Di Giuseppe, F., Bui, T. T., Vermeer, L. S., Patel, J., Scherman, D., Kichler, A., Drake, A. F., and Mason, A. J. **2012**. Control of pH responsive peptide self-association during endocytosis is required for effective gene transfer. *Biochim. Biophys. Acta* 1818:1332-1341.
- Islam, M. A., Reesor, E. K. G., Xu, Y. J., Zope, H. R., Zetter, B. R., and Shi, J. J. **2015**. Biomaterials for mRNA delivery. *Biomater. Sci.* 3:1519-1533.
- Kadlecova, Z., Baldi, L., Hacker, D., Wurm, F. M., and Klok, H. A. **2012a**. Comparative study on the in vitro cytotoxicity of linear, dendritic, and hyperbranched polylysine analogues. *Biomacromolecules* 13:3127-3137.
- Kadlecova, Z., Rajendra, Y., Matasci, M., Baldi, L., Hacker, D. L., Wurm, F. M., and Klok, H. A. **2013**. DNA delivery with hyperbranched polylysine: a comparative study with linear and dendritic polylysine. *J. Control. Release* 169:276-288.
- Kadlecova, Z., Rajendra, Y., Matasci, M., Hacker, D., Baldi, L., Wurm, F. M., and Klok, H. A. **2012b**. Hyperbranched polylysine: a versatile, biodegradable transfection agent for the production of recombinant proteins by transient gene expression and the transfection of primary cells. *Macromol. Biosci.* 12:794-804.
- Kanasty, R., Dorkin, J. R., Vegas, A., and Anderson, D. **2013**. Delivery materials for siRNA therapeutics. *Nat. Mater.* 12:967-977.
- Keles, E., Song, Y., Du, D., Dong, W.-J., and Lin, Y. **2016**. Recent progress in nanomaterials for gene delivery applications. *Biomater. Sci.* 4:1291-1309.
- Khandare, J., Calderon, M., Dagia, N. M., and Haag, R. **2012**. Multifunctional dendritic polymers in nanomedicine: opportunities and challenges. *Chem. Soc. Rev.* 41:2824-2848.
- Kodama, Y., Nakamura, T., Kurosaki, T., Egashira, K., Mine, T., Nakagawa, H., Muro, T., Kitahara, T., Higuchi, N., and Sasaki, H. **2014**. Biodegradable nanoparticles composed of dendrigraft poly-L-lysine for gene delivery. *Eur. J. Pharm. Biopharm.* 87:472-479.
- Kricheldorf, H. R. **1992**. *Handbook of Polymer Synthesis*. Marcel Dekker, New York.
- Kudsiyeva, L., Welsch, K., Campbell, F., Mohammadi, A., Dawson, N., Cui, L. L., Hailes, H. C., Lawrence, M. J., and Tabor, A. B. **2016**. Delivery of siRNA using ternary complexes containing branched cationic peptides: the role of peptide sequence, branching and targeting. *Mol. Biosyst.* 12:934-951.

- Kunal, K., Robertson, C. G., Pawlus, S., Hahn, S. F., and Sokolov, A. P. **2008**. Role of chemical structure in fragility of polymers: a qualitative picture. *Macromolecules* **41**:7232-7238.
- Le, T. C., Todd, B. D., Davis, P. J., and Uhlherr, A. **2009**. Structural properties of hyperbranched polymers in the melt under shear via nonequilibrium molecular dynamics simulation. *J. Chem. Phys.* **130**:074901.
- Leclercq, L., Boustta, M., Rixte, J., and Vert, M. **2010**. Degradability of poly(*l*-lysine) and poly(*dl*-aminoserinate) complexed with a polyanion under conditions modelling physico-chemical characteristics of body fluids. *J. Colloid Interface Sci.* **350**:459-464.
- Lee, D., Lee, Y. M., Kim, J., Lee, M. K., and Kim, W. J. **2015**. Enhanced tumor-targeted gene delivery by bioreducible polyethyleneimine tethering EGFR divalent ligands. *Biomater. Sci.* **3**:1096-1104.
- Lieber, M., Smith, B., Szakal, A., Nelson-Rees, W., and Todaro, G. **1976**. A continuous tumor-cell line from a human lung carcinoma with properties of type II alveolar epithelial cells. *Int. J. Cancer* **17**:62-70.
- Luo, X., Wang, W., Dorkin, J. R., Veiseh, O., Chang, P. H., Abutbul-Ionita, I., Danino, D., Langer, R., Anderson, D. G., and Dong, Y. **2017**. Poly(glycoamidoamine) brush nanomaterials for systemic siRNA delivery in vivo. *Biomater. Sci.* **5**:38-40.
- Midoux, P., Pichon, C., Yaouanc, J. J., and Jaffres, P. A. **2009**. Chemical vectors for gene delivery: a current review on polymers, peptides and lipids containing histidine or imidazole as nucleic acids carriers. *Br. J. Pharmacol.* **157**:166-178.
- Nasanit, R., Iqbal, P., Soliman, M., Spencer, N., Allen, S., Davies, M. C., Briggs, S. S., Seymour, L. W., Preece, J. A., and Alexander, C. **2008**. Combination dual responsive polypeptide vectors for enhanced gene delivery. *Mol. Biosyst.* **4**:741-745.
- Oupicky, D., Konak, C., Ulbrich, K., Wolfert, M. A., and Seymour, L. W. **2000**. DNA delivery systems based on complexes of DNA with synthetic polycations and their copolymers. *J. Control. Release* **65**:149-171.
- Roufai, M. B., and Midoux, P. **2001**. Histidylated polylysine as DNA vector: elevation of the imidazole protonation and reduced cellular uptake without change in the polyfection efficiency of serum stabilized negative polyplexes. *Bioconjug. Chem.* **12**:92-99.
- Samal, S. K., Dash, M., Van Vlierberghe, S., Kaplan, D. L., Chiellini, E., van Blitterswijk, C., Moroni, L., and Dubruel, P. **2012**. Cationic polymers and their therapeutic potential. *Chem. Soc. Rev.* **41**:7147-7194.
- Scholl, M., Kadlecova, Z., and Klok, H.-A. **2009**. Dendritic and hyperbranched polyamides. *Prog. Polym. Sci.* **34**:24-61.
- Scholl, M., Nguyen, T. Q., Bruchmann, B., and Klok, H.-A. **2007a**. Controlling polymer architecture in the thermal hyperbranched polymerization of *l*-lysine. *Macromolecules* **40**:5726-5734.
- Scholl, M., Nguyen, T. Q., Bruchmann, B., and Klok, H.-A. **2007b**. The thermal polymerization of amino acids revisited; synthesis and structural characterization of hyperbranched polymers from *l*-lysine. *J. Polym. Sci. A Polym. Chem.* **45**:5494-5508.
- Semple, S. C., Akinc, A., Chen, J. X., Sandhu, A. P., Mui, B. L., Cho, C. K., Sah, D. W. Y., Stebbing, D., Crosley, E. J., Yaworski, E., Hafez, I. M., Dorkin, J. R., Qin, J., Lam, K., Rajeev, K. G., Wong, K. F., Jeffs, L. B., Nechev, L., Eisenhardt, M. L., Jayaraman, M., Kazem, M., Maier, M. A., Srinivasulu, M., Weinstein, M. J., Chen, Q. M., Alvarez, R., Barros, S. A., De, S., Klimuk, S. K., Borland, T., Kosovrasti, V., Cantley, W. L., Tam, Y. K., Manoharan, M., Ciufolini, M. A., Tracy, M. A., De Fougères, A., Maclachlan, I., Cullis, P. R., Madden, T. D., and Hope, M. J. **2010**. Rational design of cationic lipids for siRNA delivery. *Nat. Biotechnol.* **28**:172-U18.
- Soliman, M., Nasanit, R., Abulateefeh, S. R., Allen, S., Davies, M. C., Briggs, S. S., Seymour, L. W., Preece, J. A., Grabowska, A. M., Watson, S. A., and Alexander, C. **2012**. Multicomponent synthetic polymers with viral-mimetic chemistry for nucleic acid delivery. *Mol. Pharm.* **9**:1-13.
- Sun, W., and Davis, P. B. **2010**. Reducible DNA nanoparticles enhance in vitro gene transfer via an extracellular mechanism. *J. Control. Release* **146**:118-127.
- Tedja, R., Marquis, C., Lim, M., and Amal, R. **2011**. Biological impacts of TiO₂ on human lung cell lines A549 and H1299: particle size distribution effects. *J. Nanopart. Res.* **13**:3801-3813.
- Udenfriend, S., Stein, S., Böhlen, P., Dairman, W., Leimgruber, W., and Weigele, M. **1972**. Fluorescamine: a reagent for assay of amino acids, peptides, proteins, and primary amines in the picomole range. *Science* **178**:871-872.
- Viricel, W., Poirier, S., Mbarek, A., Derbali, R. M., Mayer, G., and Leblond, J. **2017**. Cationic switchable lipids: pH-triggered molecular switch for siRNA delivery. *Nanoscale* **9**:31-36.
- Wagner, E. **2013**. Biomaterials in RNAi therapeutics: quo vadis? *Biomater. Sci.* **1**:804-809.
- Yang, H. H. **2006**. Polyamide fibers. in *Handbook of Fiber Chemistry*, third edn. CRC Press, Boca Raton.
- Zhang, P., and Wagner, E. **2017**. History of polymeric gene delivery systems. *Top Curr Chem (Cham)* **375**:26.
- Zhang, Y., Chan, H. F., and Leong, K. W. **2013**. Advanced materials and processing for drug delivery: the past and the future. *Adv. Drug Deliv. Rev.* **65**:104-120.
- Zhong, Z., Feijen, J., Lok, M. C., Hennink, W. E., Christensen, L. V., Yockman, J. W., Kim, Y. H., and Kim, S. W. **2005**. Low molecular weight linear polyethyleneimine-*b*-poly(ethylene glycol)-*b*-polyethyleneimine triblock copolymers: synthesis, characterization, and in vitro gene transfer properties. *Biomacromolecules* **6**:3440-3448.

Supporting information

Additional supporting information may be found online in the Supporting Information section at the end of the article.

- Figure S1: FT-IR spectra of hyperbranched polymers
 Figure S2: ¹H-NMR spectrum of *hb*-polyk
 Figure S3: ¹³C-NMR spectrum of *hb*-polyk
 Figure S4: ¹H-NMR spectrum of *hb*-polykxh
 Figure S5: ¹³C-NMR spectrum of *hb*-polykxh
 Figure S6: ¹H-NMR spectrum of polymers in group-A stacked together to show the growth in the imidazole peaks with increase in molar ratio of histidine
 Figure S7: ¹H-NMR spectrum of polymers in group-B stacked together to show the growth in the imidazole peaks with increase in molar ratio of histidine
 Figure S8: HSQC spectrum of *hb*-polyk
 Figure S9: HSQC spectrum of *hb*-polykxh
 Figure S10: Chemical shifts of imidazole amines in hyperbranched polymers at different pH values
 Figure S11: (a) The histograms of AFM images, analysed by image-j, show the size distribution of polyplexes. (b) Hydrodynamic radii of polyplexes prepared in pbs,

ph 7.4 at different n/p ratios using polymers of group-a and group-b

Figure S12: (a) Zeta potential measurements, (b) ethidium bromide displacement assay and (c) agarose gel electrophoresis of hyperbranched polymers/dna polyplexes prepared in PBS, ph 7.4 at different N/P ratios.

Figure S13: Metabolic activity of a549 cells treated with (a) the hyperbranched polymers and (b) their polyplexes

Figure S14: Luciferase activity of polyplexes prepared in PBS, ph 7.4 with polymers of high molecular weight polyplexes

Figure S15: Heparin competition assay

Figure S16: LDH assay